Computational Materials Science 117 (2016) 544–548

Contents lists available at ScienceDirect

Computational Materials Science

journal homepage: www.elsevier.com/locate/commatsci

Tunable surface-plasmon-polariton-like modes based on graphene metamaterials in terahertz region

Zehan Yao [a,c], Yuanyuan Huang [a], Qian Wang [a], Fangrong Hu [b], Baogang Quan [c], Junjie Li [c], Changzhi Gu [c], Xinlong Xu [a,*]

[a] State Key Lab Incubation Base of Photoelectric Technology and Functional Materials, International Collaborative Center on Photoelectric Technology and Nano Functional Materials, Institute of Photonics & Photon-Technology, Northwest University, Xi'an 710069, China
[b] Laboratory for Terahertz, College of Electronic Engineering and Automatization, Guilin University of Electronic Technology, Guilin 541004, China
[c] Beijing National Laboratory for Condensed Matter Physics, and Institute of Physics, Chinese Academy of Sciences, Beijing 100190, China

ARTICLE INFO

Article history:
Received 26 August 2015
Accepted 29 September 2015
Available online 17 October 2015

Keywords:
Graphene
Plasmonic metamaterials
Surface plasmon polariton
Tunability

ABSTRACT

Plasmonic response in graphene-based metamaterials show great potential for terahertz (THz) wave manipulation. In this work, we study the tunable surface-plasmon-polariton-like modes based on graphene complementary split ring resonators (CSRRs) in THz region. Our study suggests that these modes can be generated by graphene plasmonic metamaterials due to the diffraction coupling of surface plasmon and propagating electromagnetic (EM) wave. Furthermore, the modes can be tuned by stacking graphene plasmonic metamaterials layers or by changing the graphene Fermi level with electric field. Our results suggest graphene plasmonic metamaterials for both physical understanding and novel applications in THz region.

1. Introduction

Graphene, carbon atoms arranged in two dimensional honeycomb lattices, has attracted a lot of attention since its first practical production in 2004 [1]. This is mainly due to the reason that graphene has high carrier mobility [2], gate-controllable Fermi level, and broadband electromagnetic response [3], which is desirable for tunable, high-speed, and broadband optoelectronic devices. Recently, graphene has emerged as promising THz materials [3] for efficient THz wave manipulation with intrinsic plasmons, which could bridge 'THz' gap between microwave and far-infrared regions. As metamaterials afford efficient method to design and tailor nature materials, the alliance between graphene and metamaterials could further enhance optical processes of graphene. One of the promising designs is the hybridization of graphene and metamaterials, which could enhance plasmonic response for the development of THz and far-infrared detectors [4,5] and modulators [6,7]. Another method is to design metamaterials using graphene instead of noble metals in traditional metamaterials. Papasimakis et al. [8] compared single-layer graphene with single-layer of gold and proved that the magnetic response by highly doped graphene-based metamaterials is stronger than that by gold-based metamaterials. Fan et al. [9] found that the absorption in graphene can be enhanced by asymmetric split ring resonators (SRRs) in graphene-based metamaterials.

Plasmons in graphene play a pivotal role in the Dirac fermion dynamics, which have been probed by scattering-type scanning near-field optical microscope [10], and by other methods in THz and far-infrared regions [3,11]. Ju et al. [12] demonstrated light–plasmon coupling in graphene micro-ribbon array and suggested the resonant strength is quite large compared with the conventional two-dimensional electron gas in the room-temperature. Afterward, some other designs of graphene-based metamaterials such as graphene arrays [13], graphene rings [14], graphene nanodisks [15] appeared. However, these researches focused mainly on the localized surface plasmon (LSP), which can enhance the gross response of metamaterials by summing up independent localized effect. In metamaterials, the morphology of plasmonic structures could modulate the LSP and form the surface plasmon polaritons like (SPPs-like) modes, which can mimic the traditional surface plasmons [16]. In turn, these SPPs-like modes played an important role in the modulation and manipulation of electromagnetic waves for the optoelectronic devices.

In this work, we study the surface plasmon response of graphene plasmonic metamaterials based on complementary split ring resonators (CSRRs) in THz region. The plasmonic modes excited on the graphene metamaterials form the SPPs-like modes

* Corresponding author. Fax: +86 29 152 293 52076.
E-mail address: xlxuphy@nwu.edu.cn (X. Xu).

http://dx.doi.org/10.1016/j.commatsci.2015.09.063
0927-0256/

by diffraction coupling among the neighboring graphene CSRRs unit cells. We theoretically demonstrate that by the metamaterial interlayer coupling, the frequency of SPPs-like modes can shift by 14.17 THz and the resonant intensity enhance by 76% due to the strong Coulomb interaction among the adjacent graphene CSRRs layers. Furthermore, by tuning the Fermi level of graphene, the frequency of SPPs-like modes shift by 11.33 THz and the resonant intensity enhance by 41%. The graphene-based metamaterials exhibit great potential for tunable THz devices.

The sheet conductivity for single-layer graphene can be determined from the Kubo formalism [17,18]:

$$\sigma(\omega,\mu_c,\Gamma,T)=\frac{ie^2(\omega+i2\Gamma)}{\pi\hbar^2}\left[\frac{1}{(\omega+i2\Gamma)^2}\int_0^\infty E\left(\frac{\partial f_d(E)}{\partial E}-\frac{\partial f_d(-E)}{\partial E}\right)dE-\int_0^\infty\frac{\partial f_d(E)}{(\omega+i2\Gamma)^2-4(E/\hbar)^2}dE\right] \quad (1)$$

where ω is the circular frequency, μ_c is the Fermi level, E is the energy, Γ is the electron scattering rate, $\hbar$ is the reduced Plank's constant. And $f_d(\varepsilon)=(1+e^{(E-\mu_c)/K_bT})^{-1}$ is the Fermi–Dirac distribution, where e is the charge of an electron and T is temperature and K_b is Boltzmann's constant. The scattering rate Γ is proved to be independent of the Fermi level [19] (Γ^{-1} is the phenomenological electron relaxation time), which is given by $\Gamma=\mu\mu_c/eV_f^2$, and $V_f=1\times10^6$ m/s is the Fermi velocity, $\mu=20{,}000\ \mathrm{cm^2/V\,s}$ is the carrier mobility. Graphene can interact with light through intraband and interband electron transitions. In THz and far-infrared regions, the optical response is determined by intraband transition since the interband transitions are blocked. The first term in Eq. (1) is the intraband conductivity, while the second term is due to the interband contribution.

From the relationship of permittivity and conductivity, the complex permittivity of graphene can be expressed by [20]

$$\varepsilon=1+i\sigma/(\omega\varepsilon_0 t) \quad (2)$$

where $t=0.34$ nm, is the thickness of a single-layer graphene and ε_0 is the permittivity of the vacuum. ε_r is the real part of the complex permittivity, and ε_i is the imaginary part.

We studied the plasmonic response in graphene metamaterials based on the single layer CSRRs as shown in Fig. 1a. The geometrical parameter of the structure are $a=1$ μm, linewidth $w=200$ nm, and the lattice spacing $c=1.2$ μm. The graphene CSRRs is placed on a 17 nm thick quartz substrate with the permittivity 2.25. Graphene is described by a Kubo model with the Fermi level of 0.8 eV. CST MICROWAVE STUDIO was used to calculate the electromagnetic response with frequency domain solver. The simulation results shown in Fig. 1b refer to transmission spectra of the graphene plasmonic metamaterials excited by transverse electric (TE) incidence (black line) and transverse magnetic (TM) incidence (red line), respectively. The electric field is polarized along the y axis at TE incidence and along the x axis at TM incidence. TE incidence excites two plasmonic modes in 6.6 THz (r1) and 12.2 THz (r2) while another two plasmon modes in 15.9 THz (R1) and 18.8 THz (R2) are generated by TM incidence. To better understand the plasmonic resonance in graphene CSRRs, corresponding surface current are shown in Fig. 1c. It can be seen that at TE incidence, r1 has a circulating surface current which can be regarded as a magnetic plasmon mode, while r2 exhibit like a dipole mode. At TM incidence, the top and bottom polarized distribution inside the graphene CSRRs in R1 is in opposite direction and results in four directions of surface current. However, only one direction of surface current inside the graphene CSRRs has exhibited in R2, which is caused by the same orientation of the top and bottom polarization distribution. The surface current excited by TM incidence result in a quadrupole plasmon mode in R1 and a dipole plasmon mode in R2.

The dispersion of bulk plasmon can be expressed by $\omega^2=\omega_p{}^2+c^2k^2$, where ω is the wave frequency of EM wave, ω_p is the frequency of bulk plasma, c is the velocity of light in free space, and k is the wave vector of light [21]. In the presence of a planar boundary condition, a new mode, which is called surface plasmons (SPs), would emerge. Hybridization of plasmon with photon can form so-called surface plasmon polaritons (SPPs). There are mainly two cases that allow SPs to couple with light. One is the attenuated reflection using prism [22] and the other is periodic gating or surface roughness to provide a required momentum [23]. As such, metamaterials with periodic structures can support the coupling of light and plasmon to form SPPs-like modes due

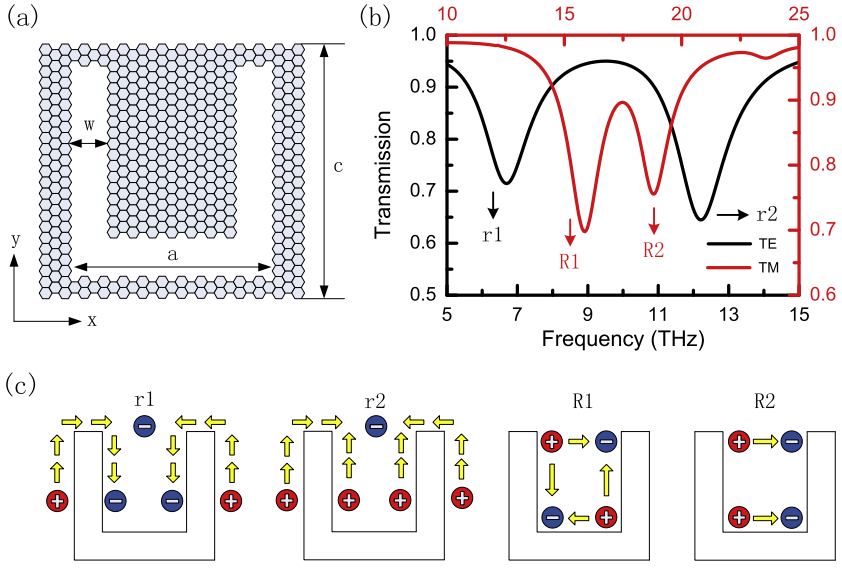

Fig. 1. (a) The 2D structure of single layer graphene CSRRs. (b) The transmission spectroscopy of single layer graphene CSRRs. The black curve including the plasmon modes of r1 and r2 refers to the simulation result at TE incidence. The red curve including the plasmon modes of R1 and R2 refers to the simulation result at TM incidence. (c) The corresponding surface current of all the plasmon modes. (For interpretation of the references to colour in this figure legend, the reader is referred to the web version of this article.)

to the effect of diffractive coupling [24]. The SPs wave vectors along the surface are modulated by the lattice constant and is proportional to the lattice constant, which can be expressed by $k = \pi/a$, where a is the lattice constant of graphene plasmonic metamaterials [25]. To investigate the SPs modes on graphene plasmonic metamaterials based on CSRRs, we set E-field monitors on each resonant frequency near the surfaces as shown in Fig. 2a–d. It can be seen that both the plasmonic modes exhibit SPPs-like electric field distribution. The complementary structure of graphene metamaterials will allow collective oscillation of carriers through E-field direction and result in SPPs-like resonance. We fit all the plasmon modes to the SPPs dispersion perfectly. The fitting results are shown in Fig. 2e and f, and will be discussed later. The SPPs-like modes propagating along the x axis can be observed at TE incidence and along the y axis can be excited by TM incidence. Interestingly, we saw another direction of SPPs-like modes along the y axis in TE incidence and can be found in r1, r2. Furthermore, all the SPPs-like modes mentioned above are limited on the interface of neighboring CSRRs unit cell. We suggest that the LSP response which is generated by the coupling of SPs and EM wave can form the SPPs-like modes by coupling among the neighboring unit cells.

To demonstrate that the plasmonic modes can couple with EM wave and form a SPPs-like dispersion, we change the unit size of single layer graphene CSRRs unit cell from 0.48 μm to 1.2 μm and keep the ratio of arm-width to arm-length constant. With the increasing of the whole unit cell, the resonant frequency of all the plasmon modes shifts toward lower frequency. This phenomenon can be explained as follows. For the electric mode, the resonant frequency is with respect to the length of the arms. With the increasing of the arm-length, the surface currents would travel more time to bypass the arms. This would raise the periodic time of the plasmon mode, and thus decrease the resonant frequency. The SPPs-like relationship can be expressed as follows [21]:

$$k^2 = \frac{\omega^2}{c^2}\left(1 + \frac{\omega^2}{\omega_p^2}\{\tanh[k_p t]\}^{-2}\right) \tag{3}$$

where k is the wave vector of SPPs-like mode, $t = 0.34$ nm is the thickness of the single-layer graphene, k_p is the wave vector of SPs and can be determined by $k_p = \omega_p/c$, ω_p is the frequency of SPs and c is the velocity of light. When $k \ll k_p$, Eq. (3) describe the dispersion relation for SPPs in thin films. Fig. 2e is the calculation data (dots) and fitting results (lines), which suggest that the dispersion features of r1, r2 in TE incidence satisfy SPPs-like dispersion relationship in Eq. (3). Furthermore, the well-fitting results of R1, R2 in TM incidence are plotted in Fig. 2f. Our fitting results demonstrate that coupling between the LSP modes in graphene metamaterials and EM wave can generate the SPPs-like modes. EM wave is scattered by one unit cell and can be collected by neighboring cells due to Coulomb interaction and carrier transfer. Our study indicated that THz EM wave can excite the SPPs-like modes propagating on the plane of graphene metamaterials.

To obtain the modulation of SPPs-like modes in graphene plasmonic metamaterials, we study the coupling of double layers graphene CSRRs. The sandwich structure shown in Fig. 3a is introduced in our simulation, indicated a 35 nm thick quartz substrate stack in the middle of two CSRRs. The dielectric constant of the quartz is 2.25. The structure parameter of CSRRs is the same as shown in Fig. 1a. Fig. 3b refers to the transmission spectra of double layers graphene CSRRs. The black curves refer to TE incidence which excites two plasmonic modes in 9.5 THz (r1) and 17.4 THz (r2). Another two plasmon modes in 22.9 THz (R1) and 27 THz (R2) are generated by TM incidence. Comparing with the transmission spectra of single layer graphene CSRRs studied in Fig. 2b, we can see that both the plasmonic modes at TE and TM incidence have blue shift. Furthermore, the resonant strength of SPPs-like modes becomes stronger. These phenomena can be explained by the strong Coulomb interaction among the adjacent layers [26]. The in-phase collective motion of carriers among the layers will lead to a stronger restoring force which is caused by the dipole–dipole coupling.

To further investigate the tunable property of graphene plasmonic metamaterials, we introduce more stacking layers of CSRRs in our simulation. As long as the several two-dimensional electron gas (2DEG) layers with the same carrier density are in the strong coupling limit, they can be regarded as a single 2DEG layer with the carrier density N times the original one 2DEG layer, where N

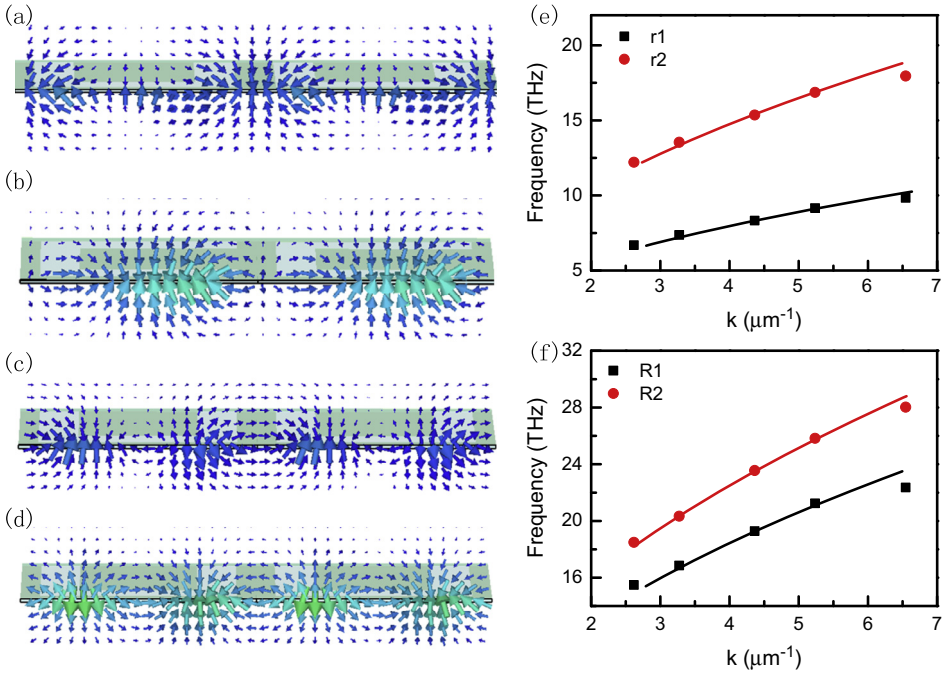

Fig. 2. The E-field cutting plane of r1 (a), r2 (b), R1 (c) and R2 (d) along x axis. The dispersion of both the resonant modes at TE incidence (e) and TM incidence (f) are fitted by the dispersion of SPPs-like modes. Dots are the simulation results and lines are the fitting results.

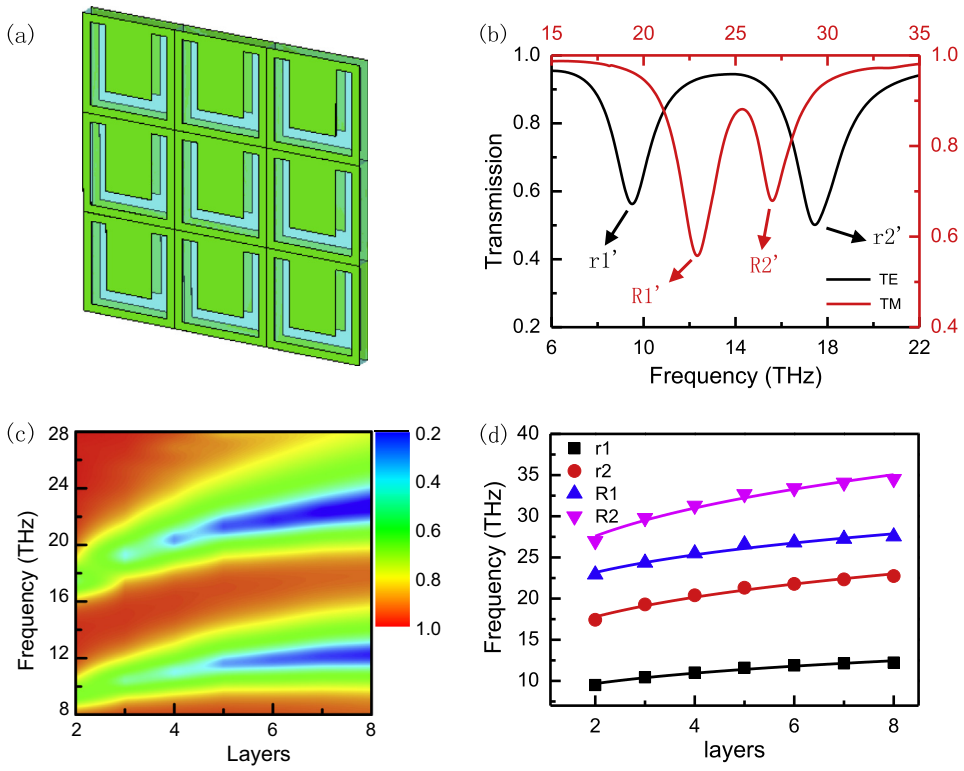

Fig. 3. (a) The 3D structure of double layer graphene CSRRs. (b) The transmission spectra of double layer graphene CSRRs. The black curve including the plasmonic modes of r1′ and r2′ refers to the simulation result at TE incidence. The red curve including the plasmonic modes of R1′ and R2′ refers to the simulation result at TM incidence. (c) Transmission spectra of CSRRs with respect to the numbers of layers at TE incidence. (d) The resonant frequency shift of all the SPPs-like modes when increasing the stacking layers from one to eight. The simulation results are fitted by $f \propto N^{\frac{1}{4}}$, where N is the number of layers. The dots are simulation results and the lines are fitting results. (For interpretation of the references to colour in this figure legend, the reader is referred to the web version of this article.)

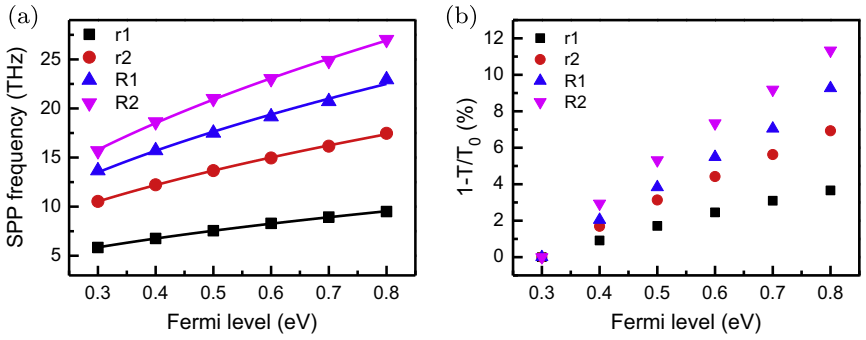

Fig. 4. (a) The frequency change of all the SPPs-like modes when increasing the graphene Fermi level from 0.3 eV to 0.8 eV. The simulation results are fitted by $f \propto \sqrt{|\mu_c|}$. The dots are simulation results and the lines are fitting results. (b) The resonant intensity enhancement ratio $1 - T/T_0$ (%) of all the SPPs-like modes when tuning the graphene Fermi level from 0.3 eV to 0.8 eV. T_0 and T refer to the SPPs-like resonant transmission with 0.3 eV and higher Fermi level graphene, respectively.

is the number of layers [27]. N times of carrier density will result in N times of restoring force and $N^{\frac{1}{4}}$ times of graphene plasmonic frequency. Since the graphene metamaterials layer spacing (35 nm) is much smaller than the unit cell parameter of the structure as shown in Fig. 3a (1.2 μm), our simulation can satisfy the strong coupling condition [28]. As shown in Fig. 3c, the stronger Coulomb interaction results in blue shift by adding the number of layers from single to eight. As such, the SPPs-like resonant strength can be significantly enhanced. Fig. 3d is the fitting results of all the SPPs-like resonances which show the blue shift with the layers. The simulation results can be well fitted by $f \propto N^{\frac{1}{4}}$. More results shown in Fig. S1 of the supplementary information indicate that the plasmonic resonant frequency can shift 4.45 THz in r1, 9.87 THz in r2, 12.39 THz in R1 and 14.17 THz in R2. At the same time, the resonant strength of SPPs-like modes can be enhanced by 62% in r1, 73% in r2, 65% in R1 and 76% in R2. These consequences demonstrate that the plasmonic coupling in the stacking layers of graphene plasmonic metamaterials can result in the increasing of carrier density and a stronger Coulomb interaction, thus leading to a significant frequency blue shift and enhance the plasmonic resonance strength of SPPs-like mode.

Graphene Fermi level can be tuned by applied gating voltage or chemical doping. This in turn will change the carrier density of graphene caused by the transition of the electrons from valence

band to conduction band and will allow the stronger interaction of the incident wave with graphene plasmonic metamaterials. As such, higher carrier density will lead to a larger resonant frequency. With the changing of Fermi level, graphene plasmonic metamaterials will show tunable electromagnetic response, which could be used to switch the EM wave [29]. To study the tunable property of the SPPs-like plasmon modes in graphene plasmonic metamaterials, we change the Fermi level from 0.3 eV to 0.8 eV. Using the same structure parameter as shown in Fig. 3(a), the transformation of SPPs-like resonant frequency and intensity as a function of Fermi level are plotted in Fig. 4. The SPPs-like resonant blue shift and become stronger with the increasing of Fermi level from 0.3 eV to 0.8 eV. The dispersion of all the SPPs-like modes as a function of graphene Fermi level can be well fitted by $f \propto \sqrt{|\mu_c|}$ [30], which is shown in Fig. 4a. And Fig. 4b shows that the resonant strength of SPPs-like modes enhance by 35% in r1, 41% in r2, 36% in R1 and 24% in R2 when increasing the graphene Fermi level from 0.3 eV to 0.8 eV. Furthermore, as shown in supply information in Fig. S2 the resonance of both the SPPs-like modes demonstrates blue shift of 3.66 THz in r1, of 6.93 THz in r2, of 9.27 THz in R1 and of 11.33 THz in R2. At the same time, the resonant intensities become stronger for both SPPs-like modes excited by the TE and TM incidence. These results are mainly due to the Fermi level dependent carrier density and suggest tunable SPPs-like modes in graphene plasmonic metamaterials for THz and far-infrared wave manipulation.

In this work, we have investigated the plasmonic modes generated by the CSRRs graphene plasmonic metamaterials. We theoretical demonstrate that the resonant modes can satisfy SPPs-like dispersion. Furthermore, we found that the frequency and resonant intensity of SPPs-like modes can be tuned by increasing the graphene plasmonic metamaterials stacking layers and by changing the graphene Fermi level. Our study suggests a tunable graphene-based plasmonic metamaterials for both physical understanding and novel applications in THz region.

Acknowledgments

This work was supported by National Natural Science Foundation of China (Nos. 11374240, 51103175, and 61265005), Ph.D. Programs Foundation of Ministry of Education of China (No. 20136101110007), Key Laboratory Science Research Plan of Shaanxi Education Department (13JS101), National Key Basic Research Program (2014CB339800).

Appendix A. Supplementary material

Supplementary data associated with this article can be found, in the online version, at http://dx.doi.org/10.1016/j.commatsci.2015.09.063.

References

[1] K.S. Novoselov, Science 306 (2004) 666–669.
[2] K.I. Bolotin, K.J. Sikes, Z. Jiang, M. Klima, G. Fudenberg, J. Hone, P. Kim, H.L. Stormer, Solid State Commun. 146 (2008) 351–355.
[3] T. Low, P. Avouris, ACS Nano 8 (2014) 1086–1101.
[4] L. Vicarelli, M.S. Vitiello, D. Coquillat, A. Lombardo, A.C. Ferrari, W. Knap, M. Polini, V. Pellegrini, A. Tredicucci, Nat. Mater. 11 (2012) 865–871.
[5] J. Li, Y. Zhou, B. Quan, X. Pan, X. Xu, Z. Ren, F. Hu, H. Fan, M. Qi, J. Bai, Carbon 78 (2014) 102–112.
[6] Y.X. Zhou, X.L. Xu, H.M. Fan, Z.Y. Ren, J.T. Bai, L. Wang, Phys. Chem. Chem. Phys. 15 (2013) 5084–5090.
[7] B. Sensale-Rodriguez, R.S. Yan, M.M. Kelly, T. Fang, K. Tahy, W.S. Hwang, D. Jena, L. Liu, H.G. Xing, Nat. Commun. 3 (2012) 780.
[8] N. Papasimakis, S. Thongrattanasiri, N.I. Zheludev, F.J. García de Abajo, Light: Sci. Appl. 2 (2013) e78.
[9] Y. Fan, Z. Wei, Z. Zhang, H. Li, Opt. Lett. 38 (2013) 5410.
[10] Z. Fei, A.S. Rodin, G.O. Andreev, W. Bao, A.S. McLeod, M. Wagner, L.M. Zhang, Z. Zhao, M. Thiemens, G. Dominguez, M.M. Fogler, A.H. Castro Neto, C.N. Lau, F. Keilmann, D.N. Basov, Nature 487 (2012) 82–85.
[11] X. Luo, T. Qiu, W. Lu, Z. Ni, Mater. Sci. Eng.: R: Rep. 74 (2013) 351–376.
[12] L. Ju, B. Geng, J. Horng, C. Girit, M. Martin, Z. Hao, H.A. Bechtel, X. Liang, A. Zettl, Y.R. Shen, Nat. Nanotechnol. 6 (2011) 630–634.
[13] M. Freitag, T. Low, W.J. Zhu, H.G. Yan, F.N. Xia, P. Avouris, Nat. Commun. 4 (2013) 1951.
[14] P. Liu, W. Cai, L. Wang, X. Zhang, J. Xu, Appl. Phys. Lett. 100 (2012) 153111.
[15] S. Thongrattanasiri, F.H. Koppens, F.J.G. de Abajo, Phys. Rev. Lett. 108 (2012) 047401.
[16] J.B. Pendry, L. Martin-Moreno, F.J. Garcia-Vidal, Science 305 (2004) 847–848.
[17] G.W. Hanson, J. Appl. Phys. 104 (2008) 084314.
[18] G.W. Hanson, J. Appl. Phys. 103 (2008) 064302.
[19] J. Horng, C.-F. Chen, B. Geng, C. Girit, Y. Zhang, Z. Hao, H.A. Bechtel, M. Martin, A. Zettl, M.F. Crommie, F. Wang, Phys. Rev. B 83 (2011) 165113.
[20] H. Ju Xu, W. Bing Lu, Y. Jiang, Z. Gao Dong, Appl. Phys. Lett. 100 (2012) 051903.
[21] E.N. Economou, Phys. Rev. 182 (1969) 539.
[22] A. Otto, Z. Phys. 216 (1968) 398.
[23] Y.Y. Teng, E.A. Stern, Phys. Rev. Lett. 19 (1967) 511.
[24] E.M. Hicks, S.L. Zou, G.C. Schatz, K.G. Spears, R.P. Van Duyne, L. Gunnarsson, T. Rindzevicius, B. Kasemo, M. Kall, Nano Lett. 5 (2005) 1065–1070.
[25] J. Zhang, C. Cao, X.L. Xu, C. Liow, S.Z. Li, P.H. Tan, Q.H. Xiong, ACS Nano 8 (2014) 3796–3806.
[26] H.G. Yan, X.S. Li, B. Chandra, G. Tulevski, Y.Q. Wu, M. Freitag, W.J. Zhu, P. Avouris, F.N. Xia, Nat. Nanotechnol. 7 (2012) 330–334.
[27] H.G. Yan, F.N. Xia, Z.Q. Li, P. Avouris, New J. Phys. 14 (2012) 125001.
[28] E.H. Hwang, S. Das Sarma, Phys. Rev. B 80 (2009) 205405.
[29] S.H. Lee, M. Choi, T.-T. Kim, S. Lee, M. Liu, X. Yin, H.K. Choi, S.S. Lee, C.-G. Choi, S.-Y. Choi, Nat. Mater. 11 (2012) 936–941.
[30] A. Grigorenko, M. Polini, K. Novoselov, Nat. Photonics 6 (2012) 749–758.